

Finite Expression Method for Learning Dynamics on Complex Networks

Zezheng Song^{*1}, Chunmei Wang^{†2}, and Haizhao Yang^{‡ 1,3}

¹Department of Mathematics, University of Maryland, College Park, MD 20742, USA

²Department of Mathematics, University of Florida, Gainesville, FL 32611, USA

³Department of Computer Science, University of Maryland, College Park, MD 20742, USA

Abstract

Complex network data pervades various real-world domains, including physical, technological, and biological systems. Despite the prevalence of such data, predicting trends and understanding behavioral patterns in complex systems remains challenging due to poorly understood underlying mechanisms. While data-driven methods have made strides in uncovering governing equations from time series data, efforts to extract physical laws from network data are limited and often struggle with incomplete or noisy data. To address these challenges, we introduce a novel approach called the Finite Expression Method (FEX) and its fast algorithm for this learning problem on complex networks. FEX represents dynamics on complex networks using binary trees composed of finite mathematical operators. The nodes within these trees are trained through a combinatorial optimization process guided by reinforcement learning techniques. This unique configuration allows FEX to capture complex dynamics with minimal prior knowledge of the system and a small dictionary of mathematical operators. Our extensive numerical experiments demonstrate that FEX excels in accurately identifying dynamics across diverse network topologies and dynamic behaviors.

Keywords Complex Networks, Network Dynamics, Finite Expression Method, High Dimensions, Symbolic Learning

1 Introduction

Complex network data is prevalent in various real-world domains, spanning from transportation [42, 61, 69, 71] to biology [11, 8, 41] and epidemiology [47, 15, 53]. For instance, proteins frequently interact with one another to execute a wide range of functions. As with many complex systems, comprehending the underlying dynamics within these networks is crucial for analyzing and predicting their behaviors. In practice, time-series data for individual nodes within a network

^{*}Email: zsong001@umd.edu.

[†]Email: chunmei.wang@ufl.edu.

[‡]Email: hzyang@umd.edu.

are often accessible. Still, extracting the dynamic interactions among these nodes to gain insights into the system’s behavior proves to be a challenging endeavor. Consequently, the physical laws governing the majority of real-world complex networks remain elusive and underexplored.

In recent years, machine learning has emerged as a promising avenue for data-driven discovery of physical laws. Notably, deep learning has demonstrated its potential to identify governing partial differential equations (PDEs) from noisy data [48, 49, 46, 64, 37, 38, 17, 55, 3, 6, 29, 12, 13, 56, 23]. The success of these methods is attributed to the expressive power of deep learning models in capturing relationships among different variables. However, there has been limited focus on the discovery of physical laws within complex networks. Discovering dynamics on network data involves various challenges:

- **Complexity and scale:** Real-world network data can be extremely large and complex, making analysis computationally expensive. In the full interaction model with N nodes in the network, each node interacts with every other particle, leading to $N(N - 1)$ interaction terms that need to be computed at each time, resulting a $O(N^2)$ complexity.
- **Data quality and availability:** The quality of network data can vary greatly. Issues like missing data, noise, and topological inaccuracies can significantly impact the analysis.

In Subsection 1.1, we summarize some of the recent work on learning dynamics from network data, and we also introduce some of the recent progress on fast algorithms. In Subsection 1.2, we introduce the overall idea of our proposed method and how it tackles these challenges.

1.1 Related work

In this Subsection, we introduce related work on identifying governing equations on network data and fast algorithms for scientific computing.

1.1.1 Discovering physical laws on network

SINDy: The Sparse Identification of Nonlinear Dynamics (SINDy) [9] algorithm aims to extract underlying governing equations from data in a interpretable and efficient way, with theoretical convergence analysis [72]. Taking time-series data as inputs, SINDy infers the underlying physical laws of the system by using Sequentially Thresholded Least Squares algorithm to choose a parsimonious model from a large library of candidate functions, usually including polynomials and trigonometric functions. SINDy has been used to identify models in fluid dynamics [24], control systems [36], and neuroscience [14], etc. However, it has been shown that the vanilla SINDy performs poorly in identifying dynamics on network data.

Two-Phase SINDy: In [26], Gao and Yan proposed a two-phase procedure consisting of global regression and local fine-tuning for graph dynamics inference. This method works by building two comprehensive function libraries, L_F and L_G , for self and interaction dynamics. Then, in the first phase, this method performs a sparse regression on the normalized input data and the libraries L_F and L_G to identify potential terms in the network dynamics. In the second phase, it performs

topological sampling to fine-tune the coefficients of functions from the first phase. This method can identify the explicit functional forms of the system dynamics, given sufficient large function libraries. However, users often lack a priori knowledge of the candidate functions, so they assume a prior solid knowledge of the system. In addition, this method is sensitive to noisy and low-resolution data because topological samplings are used in the fine-tuning stage.

Graph Neural Networks: Graph neural networks (GNNs) are popular models to learn the dynamics on the networks and make predictions on the systems [52, 70, 22, 25]. These models typically use an encoder neural network to denote node states and create a latent representation. Following this, Neural Ordinary Differential Equations (Neural ODEs) are applied on the latent space to learn the dynamics. Finally, a decoder is used to project the latent embedding back to the original high-dimensional state. While this approach is flexible enough to be applied to a wide variety of network data, it essentially functions as a “black box”, making it difficult to understand the underlying dynamics. Additionally, it struggles to generalize well to out-of-distribution data.

ARNI: Algorithm for Revealing Network Interactions (ARNI) [10] is a model-free method originally proposed to identify direct interactions of particles in a network data. It works by decomposing the dynamics of each node as a linear combination of basis functions in pairwise and higher-order interactions with other nodes in the system, and recast the reconstruction problem into a mathematical regression problem with grouped variables. Authors of [26] modified ARNI appropriately to make it capable of identifying network dynamics instead of only inferring the graph topology.

1.1.2 Fast algorithms for scientific computation

In the realm of physical sciences, it is important to develop fast and efficient algorithms to handle complex systems while keeping a high accuracy. For example, Jin et al. [35] proposed the Random Batch Methods (RBM), which splits particles in a physical system into several batches at each time to reduce the computational cost from $O(N^2)$ to $O(N)$, where N is the number of particles. In machine learning, stochastic gradient descent (SGD) [2, 7, 32] takes a random sample of the entire dataset in each iteration to compute the gradient and update model parameters. Similar to SGD, stochastic coordinate descent [44, 45] randomly samples some of the coordinates to update at each time step. In addition, randomized algorithms have been widely applied to fast matrix factorizations [18, 31, 51] and Bayesian inference [68, 50].

1.2 Our contributions

To tackle the problems seen in previous methods, we propose the finite expression method (FEX) that represents dynamics on network data by binary trees, whose nodes are mathematical operators (e.g., sin, cos, exp, etc). FEX selects the operator of each node via combinatorial optimization (CO) by a novel reinforcement learning (RL) approach. In particular, our method has major characteristics. (1) Compared to the widely used SINDy approach and its variants, FEX does not require a large library of candidate functions. In contrast, thanks to the binary tree representation, FEX can produce complicated composition of functions with a few simple mathematical operators provided by the user. (2) Our model employs a RL approach to perform operator selection in a data-driven manner (discussed in Section 3). This design has been demonstrated to promote

the expressiveness of our method of identifying network dynamics. (3) To mitigate the intensive computational burden when calculating the pair-wise interaction dynamics on network data, we employ RBM [35] to accelerate the computation while keeping a reasonable accuracy. Throughout this work, we demonstrate the advantage of our method by applying it to several synthetic complex network data to extract governing equations. An overview figure of FEX to infer physical laws on network data is provided in Fig. 1.

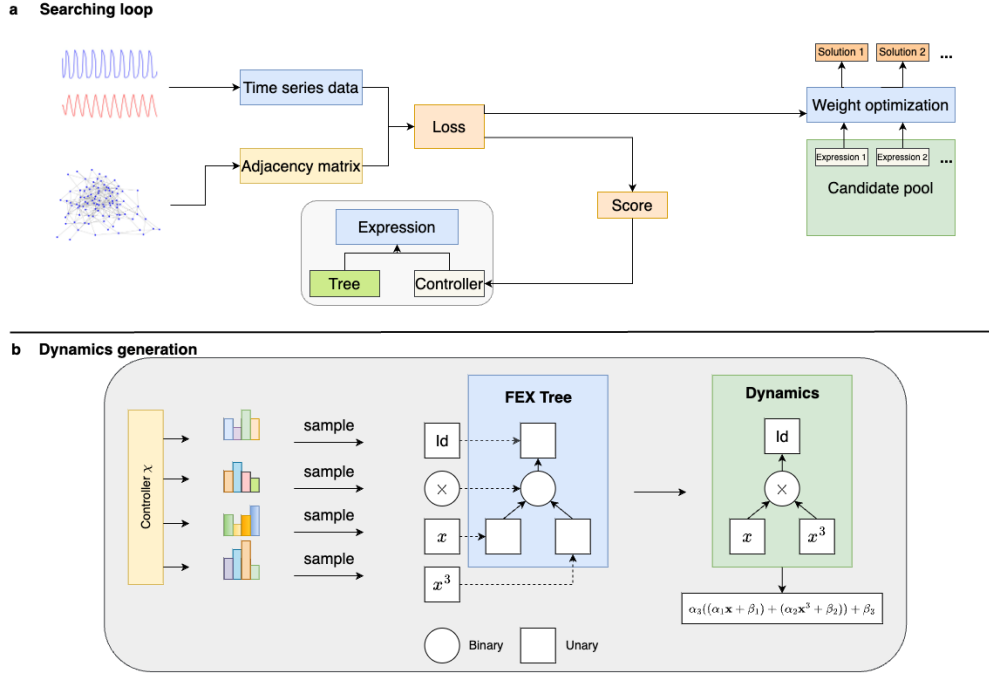


Figure 1: (A) Based on the input data of the time series and adjacency matrix, FEX performs combinatorial optimization to infer the mathematical structures of the dynamics and then implements fine-tuning on the top-performing candidates in the pool to identify the optimal dynamics. (B) FEX implements combinatorial optimization by training a controller χ to output probability mass function for each node in the FEX binary tree.

2 Problem setup

2.1 Learning dynamics on complex networks

A common model [26, 43] that describes the evolution of the states of the network of size N is given by

$$\frac{d\mathbf{x}_i(t)}{dt} = \mathbf{F}(\mathbf{x}_i(t)) + \sum_{j=1}^N \mathbf{A}_{ij} \mathbf{G}(\mathbf{x}_i(t), \mathbf{x}_j(t)), \quad (1)$$

where $\mathbf{x}_i(t) \equiv (x_{i,1}(t), \dots, x_{i,d}(t))^\top$ represents node i 's d -dimensional activity and $i = 1, \dots, N$. The dynamics of $\mathbf{x}_i(t)$ are driven by $\mathbf{F}(\mathbf{x}_i) \equiv (F_1(\mathbf{x}_i), \dots, F_d(\mathbf{x}_i))^\top$, denoting the self-dynamics, and $\mathbf{G}(\mathbf{x}_i(t), \mathbf{x}_j(t)) \equiv (G_1(\mathbf{x}_i, \mathbf{x}_j), \dots, G_d(\mathbf{x}_i, \mathbf{x}_j))^\top$, representing the interaction dynamics between any pair of nodes \mathbf{x}_i and \mathbf{x}_j . \mathbf{A}_{ij} denotes the ij -th entry in the $N \times N$ adjacency matrix \mathbf{A} , where

$\mathbf{A}_{ij} = 1$ if there is a connection between node i and node j , and $\mathbf{A}_{ij} = 0$ otherwise. Therefore, the dynamics are determined by self-dynamics, interaction dynamics and the topology of the network. However, in many real-world complex network systems, we do not have the information of the explicit forms of \mathbf{F} and \mathbf{G} . Therefore, it is important to distill the functional forms of \mathbf{F} and \mathbf{G} from node activity data, which is the focus of our work.

However, inferring underlying dynamics from real-world time series data presents a formidable challenge, primarily due to the often unclear or only partially known governing laws. The endeavor to discover dynamics within a complex network system introduces an additional layer of complexity, attributable to the interactions among entities described by the graph topology. Moreover, numerous oscillator systems exhibit varied coupling behaviors contingent upon the coupling strength between entities and the inherent graph topology, a prime example being synchronization phenomena. In addition, the data in real-world are often sparse, noisy, and come from incomplete network topology. Hence, to demonstrate the capability of FEX to discover dynamics on complex networks, we subject FEX to a rigorous examination against three classical network dynamics: Hindmarsh-Rose (HR, $d = 3$) [33, 63, 67], FitzHugh-Nagumo (FHN, $d = 2$) neuronal systems [19], and coupled heterogeneous Rössler oscillators ($d = 3$) [5], where d denotes the dimension of feature for each node. Regarding to the graph topology, we demonstrate that FEX is capable of identifying governing equations on various synthetic networks, including Erdős-Rényi (ER) [28] and scale-free (SF) [1] networks. Through this extensive examination, we aim to demonstrate the effectiveness and robustness of FEX in decoding the intricate dynamics inherent in complex network systems. Details are elaborated more in Section 4.

2.2 FEX for learning dynamics on networks

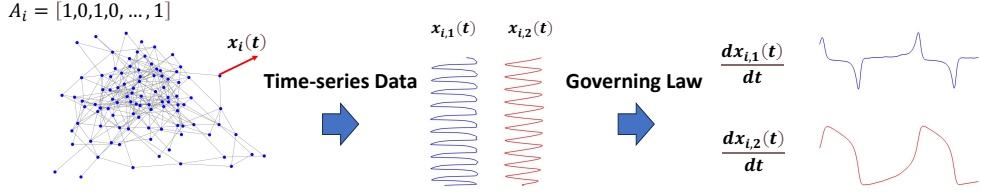
The motivation behind FEX is to develop a robust methodology for identifying physical laws from network data. Our model depicts network dynamics using two fixed-size binary trees: one representing the self-dynamics $\mathbf{F}(\mathbf{x}_i)$ while another one representing the interaction dynamics $\mathbf{G}(\mathbf{x}_i, \mathbf{x}_j)$. Each tree node denotes a simple mathematical operator—either unary (sin, cos, and exp ...) or binary (+, -, \times ...). The aim of the learning process is to identify the most suitable mathematical operator for each node of the tree, ensuring accurate representation of the dynamics. The input to FEX algorithm consists of time series data \mathbf{x}_i for each node in the network, and the adjacency matrix \mathbf{A} representing the network topology, as illustrated by Fig. 2.

2.3 Learning dynamics from sparse and noisy data

In real-world scenarios, data are inevitably contaminated by noise or by the incompleteness of network topology. Thus, evaluating the robustness of the proposed method across diverse scenarios—such as low resolution, observational noises, and spurious or missing links—is paramount. Moreover, a comparative analysis with baseline models is conducted to ascertain the relative efficacy of the proposed method.

Low resolution: Practical constraints or technological limitations often result in the collection of sparse raw data. To emulate such circumstances, we simulate nonlinear dynamics with a time step size of $t = 0.01$, followed by a uniform down-sampling of the time series data. The out-

A. Offline Stage: Data generation



B. Online Stage: Discovery of dynamics by FEX

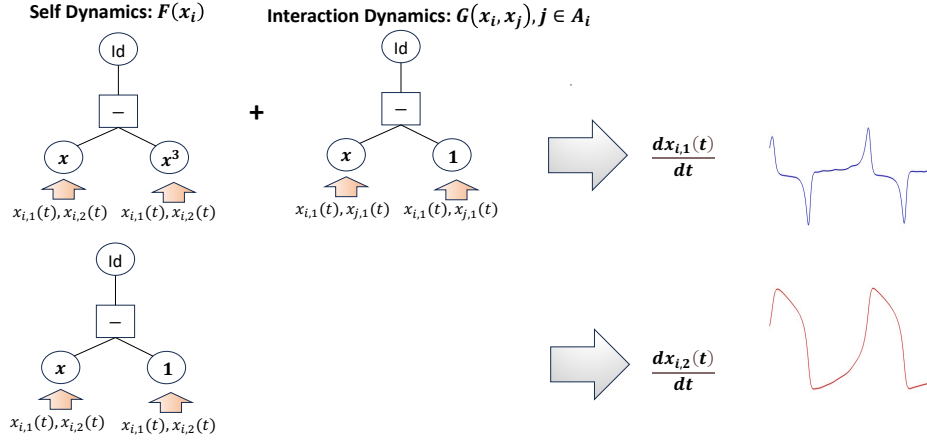


Figure 2: Representation of the components of our implementation with FHN dynamics. (A) In the offline stage, we generate time series data according to the governing law of the system, potentially with noise or low resolution. (B) In the online phase, based on the time series data, we use two FEX binary trees to infer the dynamics of the system.

comes reveal that FEX retains a high degree of accuracy, i.e., relative errors of coefficients identified by FEX and the true coefficients are less than 1%, even with merely 5% or 10% of the original data.

Spurious and missing links: In the real world, network topology may undergo evolution, making the capture of all node interactions a challenging, if not unfeasible, task. To assess the robustness of FEX against incomplete topology, we randomly either add or remove a proportion of links from the authentic network topology. The results indicate that FEX can accommodate approximately 15% missing or spurious links, showcasing its robustness in handling topological inaccuracies.

Observational noise: Observational noise is another common issue in data measurement. We replicate such noise by introducing Gaussian noises to the time series data for every node within the network. The noise intensity is modulated via the signal-to-noise ratio (SNR). The findings underscore that FEX sustains a high accuracy level, even amidst a 40-dB observational noise environment. In contrast, other baseline methods such as Two-Phase SINDy [26] and ARNI [10] identified erroneous and redundant terms with low-accurate coefficients.

Through this thorough evaluation across varied scenarios and a comparative analysis with

baseline models, we aim to demonstrate the robustness and stability of FEX in extracting dynamics from real-world, noisy data with potential topological inaccuracies. Further details are provided in Supplementary Information.

3 Methods

3.1 Overview of FEX

FEX [40, 62] introduces a novel strategy for solving PDEs and identifying physical laws from data [34]. FEX represents the system’s dynamics using a learnable binary tree to identify dynamics on network data. This tree comprises unary operators (e.g., \sin , \cos , etc.) and binary operators ($+$, $-$, \times , etc.). Additionally, each unary operator incorporates learnable weights and biases, augmenting the expressiveness of the expression. Given a specific set of operators in the tree, input variables $\mathbf{x} \in \mathbb{R}^d$ are passed through the FEX tree via the leaves. The complete FEX expression is then derived through a preorder traversal of the tree. Unlike many symbolic regression (SR) methods that generate equations autoregressively, FEX allows users to predetermine the tree’s depth and size. This distinctive feature has been demonstrated to enhance FEX’s accuracy in solving PDEs and discovering governing equations. Subsequently, with a suitable loss function, FEX conducts CO using a RL strategy to perform operator selection, and continuous optimization to refine the parameters associated with unary operators.

To address this mixed optimization problem, FEX employs a CO technique to determine the best selection of operators while leveraging a continuous optimization method to finetune the corresponding parameters of tree nodes. Regarding the CO, FEX utilizes a RL strategy to transform CO into a continuous optimization over probability distributions. To achieve this transformation, a controller network (modeled as a fully connected neural network) is integrated into FEX, which produces the probability mass function for each operator’s selection at every tree node. Consequently, selecting the most suitable operators for tree nodes is recast as the problem of training the optimal controller network capable of sampling top-performing operators. The refinement process of identifying the best controller is fundamentally a continuous optimization task. The controller network’s parameters are refined through policy gradient techniques to maximize the anticipated reward, consistent with RL conventions. As a result, the best operators can be efficiently identified by sampling from the probability distribution of the learned controller network.

In particular, analyzing dynamics in complex networks brings forth several challenges, primarily the computational complexity involved. Computing particle interactions on a graph requires $O(N^2)$ complexity, where N is the number of nodes in a network. This is prohibitive for large-scale systems. We’ve employed the RBM [35] when calculating the loss function to mitigate this. Simply put, nodes in the network are grouped into random batches and particle interactions are limited to their respective batches. By integrating RBM into the CO segment of FEX training, we’ve achieved faster computational speeds, i.e., $O(N)$ computational complexity, without sacrificing the precision required to identify the accurate structure of the FEX tree.

3.2 Functional space of finite expressions

FEX models the dynamics of network data within a functional space characterized by a finite set of operators. As such, it is crucial to clearly define this functional space where the solution resides.

Definition 3.1 (Mathematical expression [40]). A mathematical expression is a combination of symbols, which is well-formed by syntax and rules and forms a valid function. The symbols include operands (variables and numbers), operators (e.g., “+”, “sin”, integral, derivative), brackets, and punctuation.

Definition 3.2 (k -finite expression [40]). A mathematical expression is called a k -finite expression if the number of operators in this expression is k .

Definition 3.3 (Finite expression method). The finite expression method aims to numerically capture dynamics by using a limited size expression, so that the produced function closely matches the actual dynamics.

We denote \mathbb{S}_k the functional space that consists of functions formed by finite expressions with the number of operators less than or equal to k .

3.3 The combinatorial optimization problem in FEX

In FEX, the loss functional \mathcal{L} varies based on the problem. For this study, we adopt the least squares loss functional, as presented in [26], which is described as follows:

$$\mathcal{L}(F, G) = \int_0^T \left(\|\text{FEX-Tree}_F(\mathbf{x}, t) + \mathbf{A}\text{FEX-Tree}_G(\mathbf{x}, t) - \dot{\mathbf{x}}(t)\|^2 \right) dt, \quad (2)$$

where \mathbf{A} is the adjacency matrix of the network, and $\text{FEX-Tree}_F(\mathbf{x}, t)$ denotes the self-dynamics modeled by a FEX tree, $\text{FEX-Tree}_G(\mathbf{x}, t)$ denotes the interaction dynamics by another FEX tree. In FEX, the solution is found by solving the combinatorial optimization problem

$$\min_{F, G \in \mathbb{S}_{\text{FEX}}} \mathcal{L}(F, G), \quad (3)$$

where the solution space $\mathbb{S}_{\text{FEX}} \subset \mathbb{S}_k$ will be elaborated in Section 3.4.1.

3.4 Implementation of FEX

As mentioned previously, FEX’s computational process begins with the formation of a mathematical binary tree, where each node represents either a unary or a binary operator. The candidate solution u is derived from evaluating the function represented by this tree. Subsequently, the CO denoted by (3) is employed to dynamically choose the best operators for all tree nodes. This optimization aims to find operators that recover the structure of the genuine solution.

3.4.1 Finite expressions with binary trees

FEX employs a binary tree structure \mathcal{T} to represent finite expressions. The user defines the sets of potential unary and binary operators, represented by \mathbb{U} and \mathbb{B} . Common choices of unary and binary operators are respectively,

$$\sin, \exp, \text{Id}, (\cdot)^2, \int \cdot dx_i, \frac{\partial \cdot}{\partial x_i}, \dots \quad \text{and} \quad +, -, \times, \dots$$

Every unary operator in the leaf level operates on the inputs in an element-wise manner, followed by scaling parameters α_i , where $i = 1, \dots, d$, and a bias parameter β . For instance:

$$\alpha_1 \exp(x_1) + \dots + \alpha_d \exp(x_d) + \beta.$$

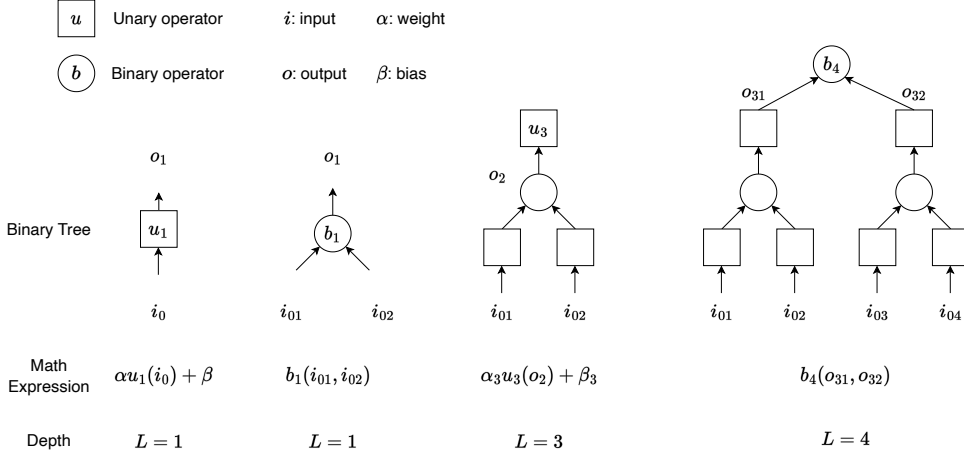


Figure 3: Computational rule of a FEX binary tree. Each unary operator is equipped with a weight α and bias β to enhance expressiveness. For tree depth greater than one (i.e., $L > 1$), the computation is implemented by recursion.

All parameters associated with unary operators are collectively represented by $\boldsymbol{\theta}$. The complete expression is derived through a preorder traversal of the operator sequence, \mathbf{e} , in the binary tree \mathcal{T} . Consequently, this finite expression is represented as $u(\mathbf{x}; \mathcal{T}, \mathbf{e}, \boldsymbol{\theta})$, as a function of input \mathbf{x} . Given a fixed \mathcal{T} , the maximum number of operators remains constrained and is upper-bounded by a constant, labeled $k_{\mathcal{T}}$. In FEX, the functional space wherein the dynamics of the system is solved is defined as:

$$\mathbb{S}_{\text{FEX}} = \{u(\mathbf{x}; \mathcal{T}, \mathbf{e}, \boldsymbol{\theta}) \mid \mathbf{e} \in \mathbb{U} \cup \mathbb{B}\}$$

The computation within the binary tree \mathcal{T} proceeds recursively, beginning at the leaf nodes. Unary operators at these leaf nodes act on the input \mathbf{x} in an element-wise manner, with the scaling factor α , transforming the dimension from \mathbb{R}^d to \mathbb{R} . Subsequently, computations proceed in a bottom-up recursive pattern until reaching the tree's root in the top level. A representation of the computation flow of such tree \mathcal{T} is presented in Fig. 3.

3.4.2 Implementation of FEX

The FEX solution represented as $u(\mathbf{x}; \mathcal{T}, \mathbf{e}, \boldsymbol{\theta})$ is derived by tackling the CO problem as:

$$\min_{\mathbf{e}, \boldsymbol{\theta}} \mathcal{L}(u(\cdot; \mathcal{T}, \mathbf{e}, \boldsymbol{\theta})). \quad (4)$$

To achieve this, FEX adopts a two-phase approach:

Operator sequence optimization: The primary goal here is to refine the operator sequence \mathbf{e} such that it reflects the structure of the authentic dynamics.

Parameter optimization: Following the sequence refinement, FEX then optimizes the parameter set $\boldsymbol{\theta}$ aiming to minimize the functional described in (4). The FEX framework is organized into four components:

- *Score Computation:* To discover the solution's structure, FEX deploys a mix-order optimization algorithm. This step assesses the score of the operator sequence \mathbf{e} . RBM is employed to accelerate the score's calculation over the network data.
- *Operator Sequence Generation:* Here, a neural network (NN) is leveraged to conceptualize a controller. This controller subsequently outputs a probability mass function, which is used for sampling optimal operator sequences.
- *Controller Update:* This step refines the parameters of the controller based on the reward outcomes of the generated operator sequences, guiding it to yield more effective sequences over training iterations.
- *Candidate Optimization:* FEX dynamically keeps a pool of the operator sequences with the highest rewards during the search process. Upon completion of training, each sequence candidate undergoes a fine-tuning phase. The ultimate objective is to identify the best operator sequence as the approximation of system dynamics.

Subsequent sections will elaborate on the details of each of these components.

3.4.3 Score computation

The evaluation of an operator sequence \mathbf{e} through its score is pivotal during training. This score guides the controller's parameter updates, aiming to produce optimal probability mass functions for the sampling of efficient operators to approximate the network dynamics. The score of \mathbf{e} , denoted as $S(\mathbf{e})$, is defined as follows:

$$S(\mathbf{e}) := (1 + L(\mathbf{e}))^{-1}, \quad \text{where} \quad L(\mathbf{e}) := \min\{\mathcal{L}(u(\cdot; \mathcal{T}, \mathbf{e}, \boldsymbol{\theta})) | \boldsymbol{\theta}\}. \quad (5)$$

For an efficient computation of the score $S(\mathbf{e})$, we employ a hybrid mix-order optimization strategy to update the parameter $\boldsymbol{\theta}$: We first take T_1 iterations using a first-order optimization algorithm, such as stochastic gradient descent [58] or Adam [39], and this yields $\boldsymbol{\theta}_{T_1}^{\mathbf{e}}$. $\boldsymbol{\theta}_{T_1}^{\mathbf{e}}$ will be used as a

warm start, followed by a T_2 iterations of a second-order optimization method, such as Newton's method [4] or BFGS [20], resulting in $\theta_{T_1+T_2}^e$.

Random Batch Method To address the computational burden when performing the total $T_1 + T_2$ optimization steps, we propose to approximate the interaction terms using only a subset of the particles at each step. In particular, we divide the N particles into n batches and only consider the interactions within each batch, then the number of interactions that need to be computed is significantly reduced. Assuming that each batch contains approximately p nodes ($n \approx \frac{N}{p}$), then the number of interactions to be computed for each batch is on the order of p^2 . Since there are n such batches, the total number of interactions at each step is on the order of $np^2 = \frac{N}{p}p^2 = Np$, which is $O(N)$ since p is a constant independent of N . This significantly reduces the computational cost when evaluating the loss function during the $T_1 + T_2$ steps of optimization.

Upon completion of these steps, the score associated with the operator sequence e is denoted as:

$$S(e) = (1 + \mathcal{L}(u(\cdot; \mathcal{T}, e, \theta_{T_1+T_2}^e)))^{-1}. \quad (6)$$

3.4.4 Operator sequence generation

The primary objective of the controller is to generate operator sequences that achieve high scores throughout the training process. We denote the controller as χ_Φ , which is parameterized by a fully connected neural network with parameters Φ . Given an operator sequence e comprising s nodes, the controller χ_Φ produces probability mass functions \mathbf{p}_Φ^i for $i = 1, \dots, s$. The operator e_j is then sampled based on the probability mass function \mathbf{p}_Φ^j . To encourage exploration within the set of operators, the ϵ -greedy strategy [65] is implemented. To be more specific, the operator e_i is selected from a uniform distribution over the entire operator set with a probability of $\epsilon < 1$.

3.4.5 Controller update

As previously discussed, we introduce a controller represented by the neural network χ_Φ , to generate a probability mass function for each node in the binary tree. This transformation changes the problem from a CO problem into a continuous optimization one. The primary goal now becomes the optimization of the controller parameters Φ so that the controller χ_Φ is capable of producing optimal probability mass function for each node. To achieve this, we consider the expected value of scores of operator sequences sampled from the controller χ_Φ , i.e.,

$$\mathcal{J}(\Phi) := \mathbb{E}_{e \sim \chi_\Phi} S(e). \quad (7)$$

The derivative of (7) with respect to Φ is

$$\nabla_\Phi \mathcal{J}(\Phi) = \mathbb{E}_{e \sim \chi_\Phi} \left\{ S(e) \sum_{i=1}^s \nabla_\Phi \log (\mathbf{p}_\Phi^i(e_i)) \right\}, \quad (8)$$

where $\mathbf{p}_\Phi^i(e_i)$ is the probability of the sampled e_i . To efficiently approximate the expectation (8), we sample a batch of operator sequences $\{\mathbf{e}^{(1)}, \mathbf{e}^{(2)}, \dots, \mathbf{e}^{(M)}\}$ each time and compute

$$\nabla_\Phi \mathcal{J}(\Phi) \approx \frac{1}{M} \sum_{k=1}^M \left\{ S(\mathbf{e}^{(k)}) \sum_{i=1}^s \nabla_\Phi \log \left(\mathbf{p}_\Phi^i(e_i^{(k)}) \right) \right\}, \quad (9)$$

where M is the batch size. Subsequently, the model parameter Φ is updated using gradient ascent, denoted as $\Phi \leftarrow \Phi + \eta \nabla_\Phi \mathcal{J}(\Phi)$. Nonetheless, the practical aim is to identify the operator sequence \mathbf{e} with the highest score, rather than optimizing the average scores of all generated operator sequences. Therefore, we follow the approach in [54] and consider

$$\mathcal{J}(\Phi) = \mathbb{E}_{\mathbf{e} \sim \chi_\Phi} \{ S(\mathbf{e}) | S(\mathbf{e}) \geq S_{\nu, \Phi} \}, \quad (10)$$

where $S_{\nu, \Phi}$ represents the $(1 - \nu) \times 100\%$ -quantile of the score distribution generated by χ_Φ . In a discrete form, the gradient computation becomes

$$\nabla_\Phi \mathcal{J}(\Phi) \approx \frac{1}{M} \sum_{k=1}^M \left\{ (S(\mathbf{e}^{(k)}) - \hat{S}_{\nu, \Phi}) \mathbf{1}_{\{S(\mathbf{e}^{(k)}) \geq \hat{S}_{\nu, \Phi}\}} \sum_{i=1}^s \nabla_\Phi \log \left(\mathbf{p}_\Phi^i(e_i^{(k)}) \right) \right\}, \quad (11)$$

where $\mathbf{1}$ denotes an indicator function which evaluates to 1 when the condition is met, and 0 otherwise. Meanwhile, $\hat{S}_{\nu, \Phi}$ represents the $(1 - \nu)$ -quantile of the scores within the set $\{S(\mathbf{e}^{(i)})\}_{i=1}^N$.

3.4.6 Candidate optimization

During the training phase of optimizing the controller parameters Φ , efficient evaluation of expressions sampled from the controller is crucial. As introduced in Section 3.4.3, this is achieved by computing the score $S(\mathbf{e})$ through $T_1 + T_2$ “coarse-tune” iterations. However, this coarse score might not reflect the performance of operator sequence \mathbf{e} owing to the optimization of a nonconvex function. Therefore, we maintain a pool \mathbb{P} with a fixed size of K during the training of controller, which dynamically holds the top-performing candidate expressions. When the controller’s training is completed, we further refine the coefficients of each candidate expression \mathbf{e} within the pool \mathbb{P} to attain high accuracy. To enhance the robustness of our method against link perturbations, we employ a random sampling strategy. In particular, for each candidate function, we perform random sampling of L times, where we randomly sample S nodes from the graph each time. For each batch, we perform T_3 iterations of optimizations based on the objective function $\mathcal{L}(u(\cdot; \mathcal{T}, \mathbf{e}, \boldsymbol{\theta}))$ with a first-order algorithm with a small learning rate, and the final coefficients $\hat{\boldsymbol{\theta}}$ of the expression are obtained by averaging the coefficients over L times.

4 Dynamics learning results

In this section, we present the results of identification of HR, FHN, and coupled Rössler dynamics with FEX on the Scale-Free (SF) network with clean data. The set up of SF network follows the description in Supplementary Information. We choose SF network since it demonstrates more complex phenomena than the ER model, and many real-world networks have scale-free property. During the offline stage, we generate the time series data with the true dynamics (ODEs). During

Dynamics	Depth of Tree
HR	4
FHN	3
Coupled Rössler	3

Table 1: Tree depth of FEX tree for each dynamics.

the inference stage, we use FEX only with the time series data to identify the governing equations of the system, without accessing to the genuine ODEs. Throughout all numerical experiments, we set the batch size in RBM as 32. In addition, we provide the depths of FEX trees used in each of the considered dynamics in the numerical examples in Table 1. Robustness analyses of FEX and other baseline methods, aimed at extracting dynamics from low-resolution data, networks with spurious or missing links, and noisy data, are discussed in the Supplementary Information.

4.1 Numerical derivatives and error metric

To approximate the time-varying derivative of each node, we apply the five-point approximation [59]

$$\dot{x}_t \approx \frac{x_{t-2\delta t} - 8x_{t-\delta t} + 8x_{t+\delta t} - x_{t+2\delta t}}{12\delta t}, \quad (12)$$

where δt is the time step.

To evaluate the accuracy of inferred dynamics, we use the metric of symmetric mean absolute percentage error (sMAPE) [21]:

$$\text{sMAPE} = \frac{1}{m} \sum_{i=1}^m \frac{|D_i - R_i|}{(|D_i| + |R_i|)}, \quad (13)$$

where m is the total number of terms of both true and inferred functions, D_i is the inferred coefficient and R_i is the true coefficient. sMAPE is an appropriate metric in evaluating the performance of baselines since it not only captures the coefficient discrepancies but also penalizes incorrect inferred terms. sMAPE ranges from 0 to 1, and the lower the value the higher the accuracy, and vice versa.

4.2 Hindmarsh-Rose dynamics

The HR model [33, 63, 67] was introduced by Hindmarsh and Rose in the early 1980s to describe neuronal activity. The HR model is a simplified model of Hodgkin-Huxley model [30] while still reproducing many of the dynamic behaviors observed in real neurons. The governing equations of HR model is given as

$$\begin{cases} \frac{dx_{i,1}}{dt} = x_{i,2} - ax_{i,1}^3 + bx_{i,1}^2 - x_{i,3} + I_{ext} + \epsilon (V_{\text{syn}} - x_{i,1}) \sum_{j=1}^N \mathbf{A}_{ij} \sigma(x_{j,1}), \\ \frac{dx_{i,2}}{dt} = c - ux_{i,1}^2 - x_{i,2}, \\ \frac{dx_{i,3}}{dt} = r [s(x_{i,1} - x_0) - x_{i,3}], \end{cases} \quad (14)$$

where the coupling term is

$$\sigma(x_{j,1}) = \frac{1}{1 + e^{-x_{j,1}}}.$$

Here $x_{i,1}$ is the membrane potential of neuron i , $x_{i,2}$ is the transport rate of ions across the membrane through the ion channels, and $x_{i,3}$ is the adaptation current. Parameters are set as: $a = 1, b = 3, c = 1, u = 5, s = 4, r = 0.004, x_0 = -1.6, \epsilon = 0.15, V_{syn} = 2$, and $I_{ext} = 3.24$ is external current. Notice that the dynamic behavior of the HR neuron can be adjusted by varying these parameters. By doing so, one can observe various neuronal activities, such as tonic spiking, phasic spiking and chaotic bursting. We generate the time series data with Equation (14), with the adjacency matrix of SF network, terminal time $T = 500$ and time step $\delta t = 0.01$.

Applying FEX to the neuronal activities data generated by HR dynamics on a directed SF network, we obtain the inferred equations as

$$\begin{cases} \frac{d\hat{x}_{i,1}}{dt} = 0.9961x_{i,2} - 1.0014x_{i,1}^3 + 2.9758x_{i,1}^2 - 0.9917x_{i,3} + 3.2392 \\ \quad + \sum_{j=1}^N \mathbf{A}_{ij} (0.2985\sigma(x_{j,1}) - 0.1477x_{i,1}\sigma(x_{j,1})), \\ \frac{d\hat{x}_{i,2}}{dt} = 1.0004 - 5.0001x_{i,1}^2 - 1.0001x_{i,2}, \\ \frac{d\hat{x}_{i,3}}{dt} = 0.0255 + 0.0182x_{i,1} - 0.0050x_{i,3}, \end{cases} \quad (15)$$

From Eq. (15), we observe that FEX not only identifies all the correct terms in the dynamics in each dimension of the node, but also learns the coefficient of each term with relative errors lower than 1%. The neuronal activities generated by FEX and true governing equations are shown in Fig. 4.

4.3 FitzHugh-Nagumo dynamics

We further test our method to the neuronal activities data generated by FHN dynamics [19]. The FHN model is another mathematical representation used to describe the spiking behavior of neurons. It is defined by a system of two ordinary differential equations, capturing the main features of excitability in nerve membrane dynamics. The equations governing the FHN neuronal network dynamics are

$$\begin{cases} \frac{dx_{i,1}}{dt} = x_{i,1} - x_{i,1}^3 - x_{i,2} - \epsilon \sum_{j=1}^N \mathbf{A}_{ij} \frac{(x_{j,1} - x_{i,1})}{k_i^{in}}, \\ \frac{dx_{i,2}}{dt} = a + bx_{i,1} + cx_{i,2}, \end{cases} \quad (16)$$

where the first component $x_{i,1}$ represents the membrane potential containing self and interaction dynamics, k_i^{in} is the in-degree of neuron i (representing the number of incoming connections to node i), and $\epsilon = 1$. The second component $x_{i,2}$ represents a recovery variable where $a = 0.28, b = 0.5$ and $c = -0.04$. We generate the time series data with Equation (16), with the adjacency matrix of SF network, terminal time $T = 300$ and time step $\delta t = 0.01$.

The equations inferred by our approach from the neuronal activities data generated on a

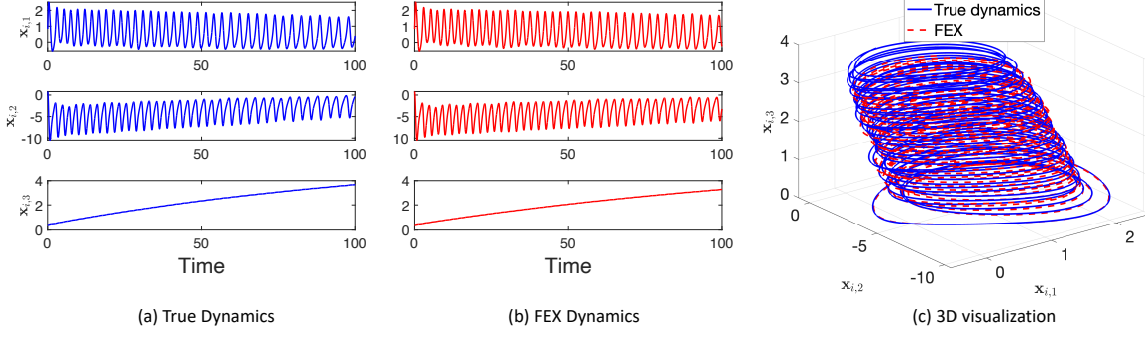


Figure 4: True HR dynamics and the dynamics identified by FEX.

directed SF network are shown below:

$$\begin{cases} \frac{d\hat{x}_{i,1}}{dt} = 0.9942x_{i,1} - 0.9998x_{i,1}^3 - 0.9999x_{i,2} - 1.0022 \sum_{j=1}^N A_{ij} \frac{(x_{j,1} - x_{i,1})}{k_i^{\text{in}}} \\ \frac{d\hat{x}_{i,2}}{dt} = 0.2801 + 0.5000x_{i,1} - 0.0400x_{i,2}. \end{cases}$$

The trajectories generated by physical laws inferred by FEX and the true governing equations are shown in Fig. 5. FEX has shown to accurately infer both dimensions of FHN system and coincide closely with the true dynamics.

4.4 Coupled Rössler dynamics

We also consider the coupled Rössler oscillators [57, 66], which is a classical model often used to study chaotic dynamics and synchronization phenomena in complex networks. We generate chaotic activities data according to the true equations governing heterogeneous Rössler dynamics [5, 60],

$$\begin{cases} \frac{dx_{i,1}}{dt} = -\omega_i x_{i,2} - x_{i,3} + \epsilon \sum_{j=1}^n A_{ij} (x_{j,1} - x_{i,1}), \\ \frac{dx_{i,2}}{dt} = \omega_i x_{i,1} + a x_{i,2}, \\ \frac{dx_{i,3}}{dt} = b + x_{i,3} (x_{i,1} + c), \end{cases} \quad (17)$$

where coupling strength $\epsilon = 0.15$, $a = 0.2$, $b = 0.2$, and $c = -5.7$. The natural frequencies of the oscillators, denoted by ω_i , follow a normal distribution with a mean value of 1 and a standard deviation of 0.1. We generate the time series data with Equation (17), with the adjacency matrix of SF network, terminal time $T = 100$ and time step $\delta t = 0.01$.

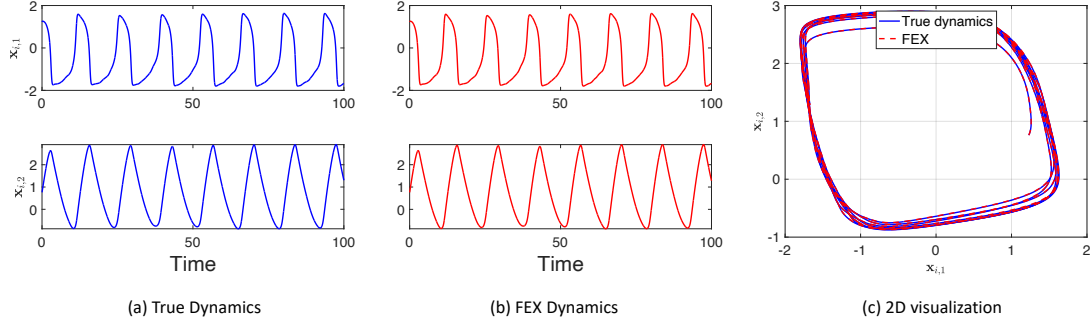


Figure 5: True FHN dynamics and the dynamics identified by FEX.

The equations inferred by FEX from the data generated on a directed SF network with $\epsilon = 0.15$ are

$$\begin{cases} \frac{d\hat{x}_{i,1}}{dt} = -1.0093x_{i,2} - 1.0027x_{i,3} + 0.1491 \sum_{j=1}^n A_{ij} (x_{j,1} - x_{i,1}), \\ \frac{d\hat{x}_{i,2}}{dt} = 0.9909x_{i,1} + 0.2030x_{i,2}, \\ \frac{d\hat{x}_{i,3}}{dt} = 0.1967 + 0.9987x_{i,3}x_{i,1} - 5.6653x_{i,3}, \end{cases} \quad (18)$$

Note that the coefficient -1.0093 of $x_{i,2}$ in the first equation of Eq. (18) and 0.9909 of $x_{i,1}$ in the second equation of Eq. (18) are estimated average value of nodes' natural frequencies, otherwise inferring a distinctive frequency for each node would lead to an n -fold increase in the dimensionality of model space. The trajectories generated by physical laws inferred by FEX and the true governing equations are shown in Fig. 6.

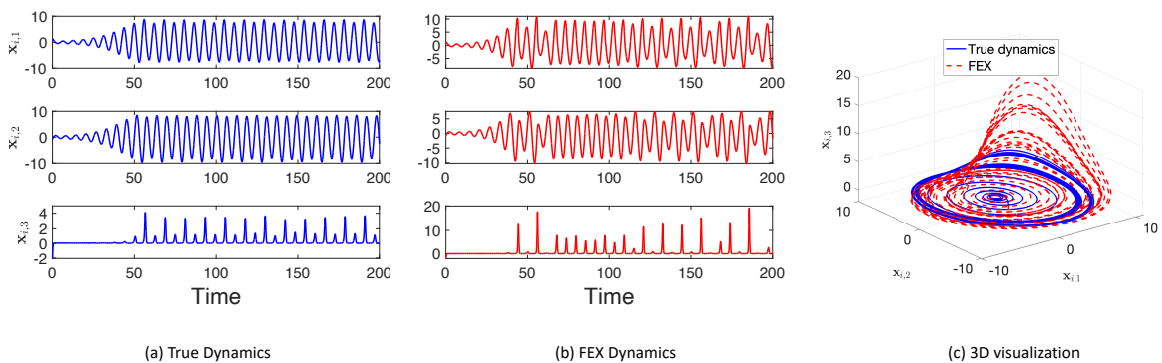


Figure 6: True coupled Rössler dynamics and the dynamics identified by FEX.

4.5 Details of performance of random batch method

As introduced before, computation on a large complex network is demanding or even infeasible. Therefore, we incorporate the RBM strategy into the FEX algorithm to accelerate the identification of the optimal mathematical structure of network dynamics while maintaining a high accuracy.

To demonstrate the efficiency of RBM in accelerating CO in the training process of FEX, we create a SF model of network size 64, 128, 256, and 512, respectively. Then, we use the time series data of FHN model on the four SF networks, and implement FEX to infer the dynamics. We record the clock time of computation of $T_1 + T_2$ coarse-tune in the FEX training algorithm by full interaction method and RBM (with a batch size of 32), respectively. The log-log plot of time vs. number of particles is shown in Fig. 7. We observe that the fitting line clock time of the full interaction model on different network sizes has a slope of approximately 2. The RBM's slope is roughly 1, indicating that the RBM demonstrates a linear scaling performance.

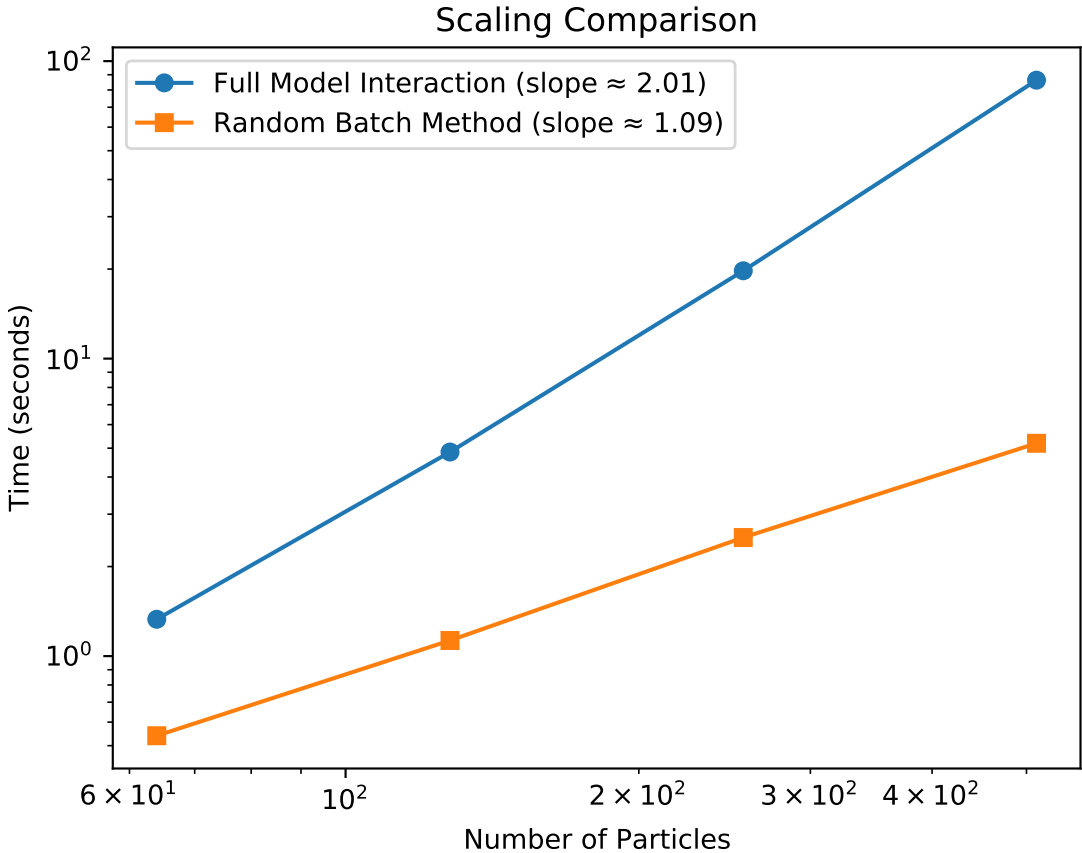


Figure 7: Clock time comparisons of full interaction model and RBM. The x -axis shows 64, 128, 256, and 512 particles of the SF network, respectively. The y -axis shows the clock time of one iteration computation for each network size.

Furthermore, we comment that we only use RBM strategy in the CO part of FEX to identify the optimal structure of the dynamics. The CO stage is the computational bottleneck of FEX,

and RBM has demonstrated its capability to determine the correct structure of dynamics while accelerating the computation significantly. After the structures of top-performing candidates are learned, we use the full interaction model in the T_3 iterations of coefficients fine-tuning stage to achieve high accuracy of dynamics inferred by FEX. The computational burden at this stage is manageable since we only have to fine-tune the coefficients of the top K candidates in the pool \mathbb{P} .

5 Conclusion

In this work, we proposed FEX as a novel methodology to learn the dynamics on complex networks. FEX has shown its capability to accurately discover physical laws on various synthetic networks, even with noise and low resolution of data. Furthermore, we incorporate RBM into our proposed FEX algorithm, which scales up FEX to handle large data when the network size increases significantly. Therefore, we have demonstrated that FEX has the potential to identify real-world dynamics in an interpretable and reliable way.

There are also questions that remained to be addressed. First, throughout our work, we consider only the pairwise interaction dynamics in the physical laws. However, it is common for complex systems to exhibit three-point or higher-order couplings among nodes in the network. Yet, it is straightforward to adapt such a setting into the FEX methodology, with the extra computational cost of including more binary trees to represent higher-order dynamics. Second, dynamics often demonstrate implicit stochasticity in real-world data, which can be described by stochastic differential equations (SDEs) [16, 27]. Lastly, this work focuses on classical dynamics with an explicit form of governing equations. However, dynamics are largely unknown or underexplored in most situations. Hence, it is interesting to observe how accurately FEX can approximate empirical dynamics and the insights it provides from inferring complex network dynamics.

References

- [1] Réka Albert and Albert-László Barabási. Statistical mechanics of complex networks. *Reviews of modern physics*, 74(1):47, 2002.
- [2] Shun-ichi Amari. Backpropagation and stochastic gradient descent method. *Neurocomputing*, 5(4-5):185–196, 1993.
- [3] Hassan Arbabi, Judith E Bunder, Giovanni Samaey, Anthony J Roberts, and Ioannis G Kevrekidis. Linking machine learning with multiscale numerics: Data-driven discovery of homogenized equations. *Jom*, 72:4444–4457, 2020.
- [4] Mordecai Avriel. *Nonlinear programming: analysis and methods*. Courier Corporation, 2003.
- [5] Baruch Barzel, Yang-Yu Liu, and Albert-László Barabási. Constructing minimal models for complex system dynamics. *Nature communications*, 6(1):7186, 2015.
- [6] Tom Bertalan, Felix Dietrich, Igor Mezić, and Ioannis G Kevrekidis. On learning hamiltonian systems from data. *Chaos: An Interdisciplinary Journal of Nonlinear Science*, 29(12), 2019.

- [7] Léon Bottou. Large-scale machine learning with stochastic gradient descent. In *Proceedings of COMPSTAT'2010: 19th International Conference on Computational StatisticsParis France, August 22-27, 2010 Keynote, Invited and Contributed Papers*, pages 177–186. Springer, 2010.
- [8] Cameron P Bracken, Hamish S Scott, and Gregory J Goodall. A network-biology perspective of microRNA function and dysfunction in cancer. *Nature Reviews Genetics*, 17(12):719–732, 2016.
- [9] Steven L Brunton, Joshua L Proctor, and J Nathan Kutz. Discovering governing equations from data by sparse identification of nonlinear dynamical systems. *Proceedings of the national academy of sciences*, 113(15):3932–3937, 2016.
- [10] Jose Casadiego, Mor Nitzan, Sarah Hallerberg, and Marc Timme. Model-free inference of direct network interactions from nonlinear collective dynamics. *Nature communications*, 8(1):2192, 2017.
- [11] Dong-Yeon Cho, Yoo-Ah Kim, and Teresa M Przytycka. Chapter 5: Network biology approach to complex diseases. *PLoS computational biology*, 8(12):e1002820, 2012.
- [12] Victor Churchill and Dongbin Xiu. Learning fine scale dynamics from coarse observations via inner recurrence. *Journal of Machine Learning for Modeling and Computing*, 3(3), 2022.
- [13] Victor Churchill and Dongbin Xiu. Flow map learning for unknown dynamical systems: overview, implementation, and benchmarks. *Journal of Machine Learning for Modeling and Computing*, 4(2), 2023.
- [14] Bryan C Daniels and Ilya Nemenman. Automated adaptive inference of phenomenological dynamical models. *Nature communications*, 6(1):8133, 2015.
- [15] Leon Danon, Ashley P Ford, Thomas House, Chris P Jewell, Matt J Keeling, Gareth O Roberts, Joshua V Ross, Matthew C Vernon, et al. Networks and the epidemiology of infectious disease. *Interdisciplinary perspectives on infectious diseases*, 2011, 2011.
- [16] Gustavo Deco, Edmund T Rolls, and Ranulfo Romo. Stochastic dynamics as a principle of brain function. *Progress in neurobiology*, 88(1):1–16, 2009.
- [17] Felix Dietrich, Alexei Makeev, George Kevrekidis, Nikolaos Evangelou, Tom Bertalan, Sebastian Reich, and Ioannis G Kevrekidis. Learning effective stochastic differential equations from microscopic simulations: Linking stochastic numerics to deep learning. *Chaos: An Interdisciplinary Journal of Nonlinear Science*, 33(2), 2023.
- [18] Petros Drineas, Ravi Kannan, and Michael W Mahoney. Fast monte carlo algorithms for matrices ii: Computing a low-rank approximation to a matrix. *SIAM Journal on computing*, 36(1):158–183, 2006.
- [19] Richard FitzHugh. Impulses and physiological states in theoretical models of nerve membrane. *Biophysical journal*, 1(6):445–466, 1961.
- [20] Roger Fletcher. *Practical methods of optimization*. John Wiley & Sons, 2013.
- [21] Benito E Flores. A pragmatic view of accuracy measurement in forecasting. *Omega*, 14(2):93–98, 1986.

[22] Cornelius Fritz, Emilio Dorigatti, and David Rügamer. Combining graph neural networks and spatio-temporal disease models to improve the prediction of weekly covid-19 cases in germany. *Scientific Reports*, 12(1):3930, 2022.

[23] Xiaohan Fu, Lo-Bin Chang, and Dongbin Xiu. Learning reduced systems via deep neural networks with memory. *Journal of Machine Learning for Modeling and Computing*, 1(2), 2020.

[24] Kai Fukami, Takaaki Murata, Kai Zhang, and Koji Fukagata. Sparse identification of nonlinear dynamics with low-dimensionalized flow representations. *Journal of Fluid Mechanics*, 926:A10, 2021.

[25] Junyi Gao, Rakshith Sharma, Cheng Qian, Lucas M Glass, Jeffrey Spaeder, Justin Romberg, Jimeng Sun, and Cao Xiao. Stan: spatio-temporal attention network for pandemic prediction using real-world evidence. *Journal of the American Medical Informatics Association*, 28(4):733–743, 2021.

[26] Ting-Ting Gao and Gang Yan. Autonomous inference of complex network dynamics from incomplete and noisy data. *Nature Computational Science*, 2(3):160–168, 2022.

[27] Mikhail Genkin, Owen Hughes, and Tatiana A Engel. Learning non-stationary langevin dynamics from stochastic observations of latent trajectories. *Nature communications*, 12(1):5986, 2021.

[28] Jesús Gómez-Gardeñes and Yamir Moreno. From scale-free to erdos-rényi networks. *Physical Review E*, 73(5):056124, 2006.

[29] Raul González-García, Ramiro Rico-Martínez, and Ioannis G Kevrekidis. Identification of distributed parameter systems: A neural net based approach. *Computers & chemical engineering*, 22:S965–S968, 1998.

[30] John Guckenheimer and Ricardo A Oliva. Chaos in the hodgkin–huxley model. *SIAM Journal on Applied Dynamical Systems*, 1(1):105–114, 2002.

[31] Nathan Halko, Per-Gunnar Martinsson, and Joel A Tropp. Finding structure with randomness: Probabilistic algorithms for constructing approximate matrix decompositions. *SIAM review*, 53(2):217–288, 2011.

[32] Moritz Hardt, Ben Recht, and Yoram Singer. Train faster, generalize better: Stability of stochastic gradient descent. In *International conference on machine learning*, pages 1225–1234. PMLR, 2016.

[33] James L Hindmarsh and RM Rose. A model of the nerve impulse using two first-order differential equations. *Nature*, 296(5853):162–164, 1982.

[34] Zhongyi Jiang, Chunmei Wang, and Haizhao Yang. Finite expression methods for discovering physical laws from data. *arXiv preprint arXiv:2305.08342*, 2023.

[35] Shi Jin, Lei Li, and Jian-Guo Liu. Random batch methods (rbm) for interacting particle systems. *Journal of Computational Physics*, 400:108877, 2020.

[36] Eurika Kaiser, J Nathan Kutz, and Steven L Brunton. Sparse identification of nonlinear dynamics for model predictive control in the low-data limit. *Proceedings of the Royal Society A*, 474(2219):20180335, 2018.

[37] George Em Karniadakis, Ioannis G Kevrekidis, Lu Lu, Paris Perdikaris, Sifan Wang, and Liu Yang. Physics-informed machine learning. *Nature Reviews Physics*, 3(6):422–440, 2021.

[38] Felix P Kemeth, Sergio Alonso, Blas Echebarria, Ted Moldenhawer, Carsten Beta, and Ioannis G Kevrekidis. Black and gray box learning of amplitude equations: Application to phase field systems. *Physical Review E*, 107(2):025305, 2023.

[39] Diederik P Kingma and Jimmy Ba. Adam: A method for stochastic optimization. *arXiv preprint arXiv:1412.6980*, 2014.

[40] Senwei Liang and Haizhao Yang. Finite expression method for solving high-dimensional partial differential equations. *arXiv preprint arXiv:2206.10121*, 2022.

[41] Gipsi Lima-Mendez and Jacques Van Helden. The powerful law of the power law and other myths in network biology. *Molecular BioSystems*, 5(12):1482–1493, 2009.

[42] Jingyi Lin and Yifang Ban. Complex network topology of transportation systems. *Transport reviews*, 33(6):658–685, 2013.

[43] Bing Liu, Wei Luo, Gang Li, Jing Huang, and Bo Yang. Do we need an encoder-decoder to model dynamical systems on networks? *arXiv preprint arXiv:2305.12185*, 2023.

[44] Ji Liu and Stephen J Wright. Asynchronous stochastic coordinate descent: Parallelism and convergence properties. *SIAM Journal on Optimization*, 25(1):351–376, 2015.

[45] Ji Liu, Steve Wright, Christopher Ré, Victor Bittorf, and Srikrishna Sridhar. An asynchronous parallel stochastic coordinate descent algorithm. In *International Conference on Machine Learning*, pages 469–477. PMLR, 2014.

[46] Yuxuan Liu, Zecheng Zhang, and Hayden Schaeffer. Prose: Predicting operators and symbolic expressions using multimodal transformers. *arXiv preprint arXiv:2309.16816*, 2023.

[47] Alun L Lloyd and Steve Valeika. Network models in epidemiology: an overview. *Complex population dynamics: nonlinear modeling in ecology, epidemiology and genetics*, pages 189–214, 2007.

[48] Zichao Long, Yiping Lu, and Bin Dong. Pde-net 2.0: Learning pdes from data with a numeric-symbolic hybrid deep network. *Journal of Computational Physics*, 399:108925, 2019.

[49] Bethany Lusch, J Nathan Kutz, and Steven L Brunton. Deep learning for universal linear embeddings of nonlinear dynamics. *Nature communications*, 9(1):4950, 2018.

[50] Yi-An Ma, Tianqi Chen, and Emily Fox. A complete recipe for stochastic gradient mcmc. *Advances in neural information processing systems*, 28, 2015.

[51] Per-Gunnar Martinsson, Vladimir Rokhlin, and Mark Tygert. A randomized algorithm for the decomposition of matrices. *Applied and Computational Harmonic Analysis*, 30(1):47–68, 2011.

[52] Charles Murphy, Edward Laurence, and Antoine Allard. Deep learning of contagion dynamics on complex networks. *Nature Communications*, 12(1):4720, 2021.

[53] Romualdo Pastor-Satorras, Claudio Castellano, Piet Van Mieghem, and Alessandro Vespignani. Epidemic processes in complex networks. *Reviews of modern physics*, 87(3):925, 2015.

[54] Brenden K Petersen, Mikel Landajuela Larma, Terrell N. Mundhenk, Claudio Prata Santiago, Soo Kyung Kim, and Joanne Taery Kim. Deep symbolic regression: Recovering mathematical expressions from data via risk-seeking policy gradients. In *International Conference on Learning Representations*, 2021.

[55] Yorgos M Psarellis, Seungjoon Lee, Tapomoy Bhattacharjee, Sujit S Datta, Juan M Bello-Rivas, and Ioannis G Kevrekidis. Data-driven discovery of chemotactic migration of bacteria via machine learning. *arXiv preprint arXiv:2208.11853*, 2022.

[56] Tong Qin, Kailiang Wu, and Dongbin Xiu. Data driven governing equations approximation using deep neural networks. *Journal of Computational Physics*, 395:620–635, 2019.

[57] Michael G Rosenblum, Arkady S Pikovsky, and Jürgen Kurths. Phase synchronization of chaotic oscillators. *Physical review letters*, 76(11):1804, 1996.

[58] David E Rumelhart, Geoffrey E Hinton, and Ronald J Williams. Learning representations by back-propagating errors. *nature*, 323(6088):533–536, 1986.

[59] Timothy Sauer. Numerical solution of stochastic differential equations in finance. In *Handbook of computational finance*, pages 529–550. Springer, 2011.

[60] Michael Schmidt and Hod Lipson. Distilling free-form natural laws from experimental data. *science*, 324(5923):81–85, 2009.

[61] Harold Soh, Sonja Lim, Tianyou Zhang, Xiuju Fu, Gary Kee Khoon Lee, Terence Gih Guang Hung, Pan Di, Sylvester Prakasam, and Limsoon Wong. Weighted complex network analysis of travel routes on the singapore public transportation system. *Physica A: Statistical Mechanics and its Applications*, 389(24):5852–5863, 2010.

[62] Zezheng Song, Maria K Cameron, and Haizhao Yang. A finite expression method for solving high-dimensional committor problems. *arXiv preprint arXiv:2306.12268*, 2023.

[63] Marco Storace, Daniele Linaro, and Enno de Lange. The hindmarsh–rose neuron model: bifurcation analysis and piecewise-linear approximations. *Chaos: An Interdisciplinary Journal of Nonlinear Science*, 18(3), 2008.

[64] Yifan Sun, Linan Zhang, and Hayden Schaeffer. Neupde: Neural network based ordinary and partial differential equations for modeling time-dependent data. In *Mathematical and Scientific Machine Learning*, pages 352–372. PMLR, 2020.

[65] Richard S Sutton and Andrew G Barto. *Reinforcement learning: An introduction*. MIT press, 2018.

[66] Longkun Tang, Xiaoqun Wu, Jinhu Lü, Jun-an Lu, and Raissa M D’Souza. Master stability functions for complete, intralayer, and interlayer synchronization in multiplex networks of coupled rössler oscillators. *Physical Review E*, 99(1):012304, 2019.

[67] X-J Wang. Genesis of bursting oscillations in the hindmarsh-rose model and homoclinicity to a chaotic saddle. *Physica D: Nonlinear Phenomena*, 62(1-4):263–274, 1993.

[68] Max Welling and Yee W Teh. Bayesian learning via stochastic gradient langevin dynamics. In *Proceedings of the 28th international conference on machine learning (ICML-11)*, pages 681–688, 2011.

- [69] Zengwang Xu and Robert Harriss. Exploring the structure of the us intercity passenger air transportation network: a weighted complex network approach. *GeoJournal*, 73:87–102, 2008.
- [70] Chengxi Zang and Fei Wang. Neural dynamics on complex networks. In *Proceedings of the 26th ACM SIGKDD international conference on knowledge discovery & data mining*, pages 892–902, 2020.
- [71] Massimiliano Zanin, Xiaoqian Sun, and Sebastian Wandelt. Studying the topology of transportation systems through complex networks: handle with care. *Journal of Advanced Transportation*, 2018, 2018.
- [72] Linan Zhang and Hayden Schaeffer. On the convergence of the sindy algorithm. *Multiscale Modeling & Simulation*, 17(3):948–972, 2019.

Acknowledgments C. W. was partially supported by National Science Foundation under award DMS-2206332. H. Y. was partially supported by the US National Science Foundation under awards DMS-2244988, DMS-2206333, and the Office of Naval Research Award N00014-23-1-2007.

Competing interests The authors declare no competing interests.

1 Supplementary Information for:

2 Finite expression method to learn dynamics on complex networks

3 Zezheng Song^{*1}, Chunmei Wang^{†2}, and Haizhao Yang^{‡ 1,3}

4 ¹Department of Mathematics, University of Maryland, College Park, MD 20742, USA

5 ²Department of Mathematics, University of Florida, Gainesville, FL 32611, USA

6 ³Department of Computer Science, University of Maryland, College Park, MD 20742, USA

7 Contents

8	A Networks	1
9	B Algorithm and experimental details	3
10	C Robustness analyses	3
11	C.1 Low resolution by experimental techniques	4
12	C.2 Spurious and missing links	5
13	C.3 Observational noises	6

14 A Networks

15 In our work, we consider several synthetic networks to demonstrate the capabilities of FEX to
16 identify dynamics on various network topologies.

17 **Erdős-Rényi (ER) model:** ER model [?, ?] is one of the foundational models for random
18 graphs. It is used widely to understand the properties of complex networks in various fields, such
19 as sociology, biology, and technology. In a ER model, a graph is constructed by connecting nodes
20 randomly with a probability of p . We generate ER networks by using the *erdos_renyi_graph(n,p)*
21 in *networkX* [?], where $n = 100, p = 0.05$. Here, n denotes the number of nodes in the graph and p

^{*}Email: zsong001@umd.edu.

[†]Email: chunmei.wang@ufl.edu.

[‡]Email: hzyang@umd.edu.

22 represents the probability to connect two arbitrary nodes, respectively. This set up results a graph
 23 with an average degree of $\langle k \rangle = 4.95$. To create a directed graph based on ER model, we allocate
 24 the direction of the link, i.e., from i to j , from j to i , or a reciprocal connection between them
 25 (both i to j and j to i directions exist), with an equal likelihood (each of probability $\frac{1}{3}$).

26 **Scale-Free (SF) network:** SF networks are ubiquitous in real-world applications [?]. This
 27 type of network demonstrates an interesting phenomenon: nodes with more early connections tend
 28 to attract even more connections, leading to the “rich get richer” scenario. Therefore, the network’s
 29 degree follows a power law distribution, implying a few nodes with very high degrees (hubs) and
 30 many with low degrees. Networks structured according to the scale-free model are constructed
 31 utilizing the Barabási-Albert (BA) [?, ?, ?] framework. Initially, we build such network by building
 32 a complete graph of a small number m_0 of nodes. Then at each time step, we add a new node
 33 with $m \leq m_0$ edges. The probability that the new node will connect to node i is $P(i) = \frac{k_i}{\sum_j k_j}$,
 34 where k_i is the degree of node i , and the sum is over all existing nodes j . Therefore, when the new
 35 node is added, it has a higher probability of connecting to nodes with high degrees, known as the
 36 “preferential attachment”. We use the *barabasi_albert_graph* function (with parameters $n = 100$,
 37 $m = 5$) in *NetworkX* to generate SF network, where n is the number of nodes in the graph, and m
 38 denotes each node connects to m existing nodes. Initially, every link is established as bidirectional.
 39 Subsequently, a select portion of these unidirectional links are randomly removed, albeit with the
 40 stipulation of maintaining a weakly connected network architecture. The result is a directed SF
 41 network with an average total degree of $\langle k \rangle = 5.1$. An illustration of the ER model and the SF
 42 network is provided in Supplementary Fig. 1.

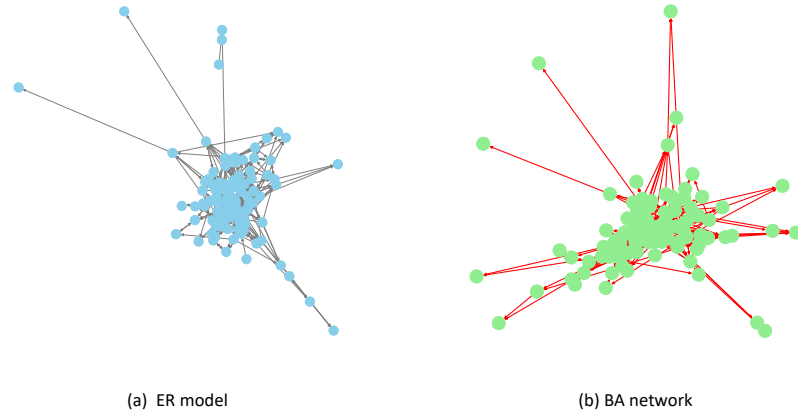


Figure 1: Visualization of ER model and SF (BA) network. (a) In ER network, the graph is essentially random without any structures or patterns. (b) In SF (BA) network, nodes closer to the boundary have generally low degrees, while there are some interior nodes with a high number of connections (hubs).

43 Despite being synthetic, the ER model and the SF network are classic and essential network
 44 models within the scientific community. Given that numerous real-world networks exhibit scale-free
 45 properties, the ability of FEX to identify physical laws on such networks accurately holds significant
 46 potential for applications in real-world data.

47 **B Algorithm and experimental details**

48 In this section, we provide an overview of the implementation details of FEX of identification of
49 network dynamics. The training algorithm of FEX is summarized in Supplementary Algorithm 1.
50 The details of hyperparameters in the algorithm are introduced as follows.

51 (1) *Score computation.* The score of an operator sequence \mathbf{e} is updated with the Adam
52 optimizer with a learning rate of 0.001 across T_1 iterations. Following this initial phase, refinement
53 of the score is carried out through the BFGS optimizer with learning rate of 1, for up to 20 iterations.

54 (2) *Operator sequence generation.* In FEX framework, a binary tree of variable depths is
55 utilized, where the binary operator set is chosen as $\mathbb{B} = \{+, -, \times\}$, and the unary operator set
56 as $\mathbb{U} = \{0, 1, \text{Id}, (\cdot)^2, (\cdot)^3, (\cdot)^4, \exp, \sin, \cos, \tanh, \text{sigmoid}\}$. The controller χ_Φ is parameterized as
57 a neural network with parameter Φ . It takes a constant input of dimension 20, while the output
58 size is determined by the expression $n_1|\mathbb{B}| + n_2|\mathbb{U}|$. Within this expression, n_1 and n_2 denote the
59 counts of binary and unary operators, respectively, and $|\cdot|$ denotes the cardinality of a set.

60 (3) *Controller update.* The update of policy gradient is implemented with a batch size of
61 $M = 10$ over 300 iterations with the Adam optimizer at a learning rate of 0.002. To encourage the
62 exploration of new operators, the ϵ -greedy strategy is employed, wherein the probability of random
63 sampling for an \mathbf{e}_i is fixed at 0.1.

64 (4) *Candidate optimization.* The capacity of the candidate pool is denoted by $K = 15$. For
65 every \mathbf{e} belonging to the set \mathbb{P} , the parameter θ is optimized via the Adam optimizer, initiated at
66 a learning rate of 0.001 across 20,000 iterations. The learning rate follows a cosine decay schedule
67 as in [?]. The number of sampling is chosen as $L = 5$, and each random sample contains $S = 20$
68 nodes.

69 **C Robustness analyses**

70 In practical situations, data are often of low resolution and noisy. To evaluate the robustness of
71 our proposed method, we perform a series of tests under various conditions: low data resolution,
72 spurious or missing connections within the graph structure, and noisy data. To mimic a low-
73 resolution data scenario, we down-sample the time series of all nodes within the complex network
74 regularly. A random set of edges within the graph is either inserted or removed to emulate situations
75 with spurious or missing connections. Gaussian noise is integrated into the time series data when
76 simulating noise corruption. This comprehensive testing framework aims to show that our method
77 demonstrates robust performance across a range of realistic and noisy data environments. In
78 the following subsections, we elaborate on each of the tests respectively. We use Two-Phase and
79 ARNI as our baselines for inferring dynamics on complex network. Both of them require two
80 comprehensive libraries, L_F (self-dynamics) and L_G (interaction dynamics). We summarize them
81 in Supplementary Table 1 and Supplementary Table 2, respectively.

Algorithm 1 Fast FEX algorithm with RBM to identify dynamics on networks

Input: Adjacency matrix \mathbf{A} of network; Time series data \mathbf{x} of time steps T_s of N nodes in the network; Loss functional \mathcal{L} ; self-dynamics tree \mathcal{T}_1 ; Interaction dynamics tree \mathcal{T}_2 ; Searching loop iteration T ; Coarse-tune iteration T_1 with Adam; Coarse-tune iteration T_2 with BFGS; Fine-tune iteration T_3 with Adam; Pool size K ; Batch size M ; Coefficient filtering threshold τ ; Number of sampling L ; Sampling batch size S ;

Output: The solution $u(\mathbf{x}; \mathcal{T}_1, \mathcal{T}_2, \hat{\mathbf{e}}, \hat{\mathbf{f}}, \hat{\boldsymbol{\theta}}_1, \hat{\boldsymbol{\theta}}_2)$.

```
1: Initialize the agent  $\chi_{\phi,1}$  and  $\chi_{\phi,2}$  for tree  $\mathcal{T}_1$ , and  $\mathcal{T}_2$ , respectively
2:  $\mathbb{P} \leftarrow \{\}$ ,
3: for  $t$  from 1 to  $T$  do
4:   Sample  $M$  operator sequences  $\{\mathbf{e}^{(1)}, \mathbf{e}^{(2)}, \dots, \mathbf{e}^{(M)}\}$  from  $\chi_{\phi,1}$ 
5:   Sample  $M$  operator sequences  $\{\mathbf{f}^{(1)}, \mathbf{f}^{(2)}, \dots, \mathbf{f}^{(M)}\}$  from  $\chi_{\phi,2}$ 
6:   for  $m$  from 1 to  $M$  do
7:     Divide  $\{1, 2, \dots, N\}$  into  $n$  batches randomly
8:     for each batch  $\mathcal{C}_q$  do
9:       Compute the loss of particle  $i$  ( $i \in \mathcal{C}_q$ ) by

$$\frac{1}{T_s} \sum_{t=1}^{T_s} \left( \left\| \mathcal{T}_1(x_i, t) + \sum_{j \in \mathcal{C}_q} \mathbf{A}_{ij} \mathcal{T}_2(x_i, t) - \dot{\mathbf{x}}_i(t) \right\|^2 \right)$$

10:    end for
11:    Optimize  $\mathcal{L}(u(\mathbf{x}; \mathcal{T}_1, \mathcal{T}_2, \mathbf{e}^{(m)}, \mathbf{f}^{(m)}, \boldsymbol{\theta}_1, \boldsymbol{\theta}_2))$  by coarse-tune with  $T_1 + T_2$  iterations.
12:    Compute the reward  $R(\mathbf{e}^{(m)}, \mathbf{f}^{(m)})$  of  $\mathbf{e}^{(m)}$  and  $\mathbf{f}^{(m)}$ 
13:    if  $\mathbf{e}^{(m)}$  and  $\mathbf{f}^{(m)}$  belongs to the top- $K$  of candidates then
14:       $\mathbb{P}.\text{append}(\mathbf{e}^{(m)} \text{ and } \mathbf{f}^{(m)})$ 
15:       $\mathbb{P}$  pops some  $\mathbf{e}$  and  $\mathbf{f}$  with the smallest reward when overloading
16:    end if
17:  end for
18:  Update  $\chi_{\phi,1}$  from Section 3.4.5
19:  Update  $\chi_{\phi,2}$  from Section 3.4.5
20: end for
21: for  $\mathbf{e}$  and  $\mathbf{f}$  in  $\mathbb{P}$  do
22:   for  $l$  from 1 to  $L$  do
23:     Randomly sample  $S$  nodes from the total  $N$  nodes;
24:     Fine-tune  $\mathcal{L}(u(\mathbf{x}^S; \mathcal{T}_1, \mathcal{T}_2, \mathbf{e}, \mathbf{f}, \boldsymbol{\theta}_1^S, \boldsymbol{\theta}_2^S))$  with  $T_3$  iterations, apply coefficient filtering with threshold  $\tau$ .
25:   end for
26:   average  $\boldsymbol{\theta}_1^S, \boldsymbol{\theta}_2^S$  over  $L$  runs to obtain  $\hat{\boldsymbol{\theta}}_1, \hat{\boldsymbol{\theta}}_2$ ;
27: end for
28: return the expression with the smallest fine-tune error.
```

⁸² **C.1 Low resolution by experimental techniques**

⁸³ In this subsection, we test the robustness of FEX with low resolution data. We test this on
⁸⁴ the Coupled Rössler dynamics on the directed SF network. To be more specific, we systematically
⁸⁵ perform down-sampling on the time series data of each node within the network, aiming to evaluate

Functions	L_F
Polynomial	x_i, x_i^2, x_i^3, x_i^4
Exponential	$\exp(x_i)$
Activation	$\sigma(x_i), \tanh(x_i)$
Rescaling	$\frac{x_i}{k_i^{\text{in}}}$
Trigonometric	$\sin(x_i), \cos x_i$

Table 1: Library functions (Two-Phase and ARNI) for self-dynamics.

Functions	$L_G(x_j)$	$L_G(x_i x_j)$	$L_G(x_j - x_i)$	$x_i L_G(x_j)$
Polynomial	x_j, x_j^2	$x_i x_j, (x_i x_j)^2$	$x_j - x_i, (x_j - x_i)^2$	$x_i x_j^2$
Exponential	$\exp(x_j)$	$\exp(x_i x_j)$	$\exp(x_j - x_i)$	$x_i \exp(x_j)$
Activation	$\tanh(x_j), \sigma(x_j)$	$\tanh(x_i x_j), \sigma(x_i x_j)$	$\tanh(x_j - x_i), \sigma(x_j - x_i)$	$x_i \tanh(x_j), x_i \sigma(x_j)$
Rescaling	$\frac{x_j}{k_i^{\text{in}}}$	$\frac{x_i x_j}{k_i^{\text{in}}}$	$\frac{x_j - x_i}{k_i^{\text{in}}}$	$\frac{x_i x_j}{k_i^{\text{in}}}$
Trigonometric	$\sin(x_j), \cos(x_j)$	$\sin(x_i x_j), \cos(x_i x_j)$	$\sin(x_j - x_i), \cos(x_j - x_i)$	$x_i \sin(x_j), x_i \cos(x_j)$

Table 2: Library functions (Two-Phase and ARNI) for interaction dynamics.

86 the impact of reduced data resolution on our methodology. Specifically, we apply two distinct down-
87 sampling rates of 10% and 5%. This process allows us to emulate scenarios of considerably lower
88 data resolution, enabling an assessment of our method’s performance and robustness under such
89 constrained data conditions.

90 The dynamics of the first dimension of Coupled Rössler dynamics identified by Two-Phase,
91 ARNI and FEX are summarized in Supplementary Table 3 and Supplementary Table 4 with down-
92 sampling rates 10% and 5%, respectively. It can be observed that FEX consistently achieves better
93 coefficient identification accuracies under different sampling rates, especially in the coefficients
94 of interaction dynamics $\mathbf{G}(x_i, x_j)$. The sMAPEs of all compared methods with different down-
95 sampling rates are summarized in Supplementary Table 5.

96 C.2 Spurious and missing links

97 In real-world scenarios, accurately observing the topology of networks is often impractical, so a thor-
98ough evaluation of our method’s robustness in the presence of spurious or missing links is necessary.
99 Therefore, we select directed SF networks as our testbed, wherein we introduce perturbations by

	True Dynamics	Two-Phase	ARNI	FEX
$\mathbf{F}(x_i)$	$-\omega_i x_{i,2}$ $-x_{i,3}$	$-1.0113 x_{i,2}$ $-0.9783 x_{i,3}$	$-1.0123 x_{i,2}$ $-0.9625 x_{i,3}$	$-1.0045 x_{i,2}$ $-0.9991 x_{i,3}$
$\mathbf{G}(x_i, x_j)$	$0.15(x_{j,1} - x_{i,1})$	$0.0973(x_{j,1} - x_{i,1})$	$0.1263(x_{j,1} - x_{i,1})$	$0.1431(x_{j,1} - x_{i,1})$

Table 3: Numerical results for coupled Rössler dynamics (down-sampling rate 10%) in self-dynamics $\mathbf{F}(x_i)$ and interaction dynamics $\mathbf{G}(x_i, x_j)$ term by term.

	True Dynamics	Two-Phase	ARNI	FEX
$\mathbf{F}(x_i)$	$-\omega_i x_{i,2}$	$-1.0114 x_{i,2}$	$-1.0275 x_{i,2}$	$-1.0063 x_{i,2}$
	$-x_{i,3}$	$-0.9251 x_{i,3}$	$-0.9338 x_{i,3}$	$-0.9741 x_{i,3}$
$\mathbf{G}(x_i, x_j)$	$0.15(x_{j,1} - x_{i,1})$	$0.0826(x_{j,1} - x_{i,1})$	$0.1045(x_{j,1} - x_{i,1})$	$0.1348(x_{j,1} - x_{i,1})$

Table 4: Numerical results for coupled Rössler dynamics (down-sampling rate 5%) in self-dynamics $\mathbf{F}(x_i)$ and interaction dynamics $\mathbf{G}(x_i, x_j)$ term by term.

Down-sampling rate	Two-Phase	ARNI	FEX
10%	0.0765	0.0370	0.0087
5%	0.1114	0.0755	0.0232

Table 5: sMAPE of Coupled Rössler dynamics with low resolution data.

100 randomly adding or removing certain edges. Consequently, during offline phase, we generate the
101 time series data with the true adjacency matrix of the SF network. During the online phase, we
102 use perturbed network adjacency matrix to infer the underlying physical laws of the system. In
103 particular, we randomly add or remove 15% links in the underlying SF networks, respectively. The
104 dynamics identified by Two-Phase, ARNI and FEX are summarized in Supplementary Table 6 and
105 Supplementary Table 7, respectively. We note that FEX exhibits robustness against graph pertur-
106 bations, in scenarios of both spurious and missing links, attributed to its design which aims to limit
107 the size of the generated expressions and the fine-tuning of parameters. The Two-Phase method is
108 comparable to FEX, and shows decent robustness against graph topology perturbations, owing to
109 its topological sampling in the second phase. On the contrary, ARNI falls short in performance on
110 noisy network structures as it was initially proposed to infer network topology, thereby potentially
111 leading to overfitting. ARNI infers many redundant terms in the dynamics with highly inaccurate
112 coefficients of each term. The sMAPEs of all compared methods with 15% spurious and missing
113 links are summarized in Supplementary Table 8.

114 C.3 Observational noises

115 In this subsection, we demonstrate the robustness of our method against observational noises. We
116 focus on the HR dynamics on a directed SF network. We generate noisy data through

$$X_i^{obs}(t) = \mathbf{x}_i(t) + a\beta_X(t),$$

117 where $\beta_X(t)$ is observational noise, which follows a Gaussian distribution with zero mean and
118 standard deviation one, so the parameter a is used to tune the level of noise.

119 From Supplementary Table 9, Supplementary Table 10 and Supplementary Table 11, FEX
120 demonstrates its capability to accurately identify all terms within the HR dynamics with their
121 respective coefficients with $SNR = 45$ and 40 . The Two-Phase method can indeed infer the correct
122 terms in the dynamics in the case of $SNR = 45$. However, the accuracy of inferred coefficients is
123 low, particularly in the interaction dynamics. In addition, in the case of $SNR = 40$, Two-Phase
124 method fails to infer the $-0.15x_{i,1}\sigma(x_{j,1})$ term in the interaction dynamics. ARNI can infer most

	True Dynamics	Two-Phase	ARNI	FEX
$\mathbf{F}(x_i)$	$x_{i,1}$	$0.9897x_{i,1}$	$6.8282x_{i,1}$	$0.9807x_{i,1}$
	$-x_{i,1}^3$	$-0.9733x_{i,1}^3$	$-0.1202x_{i,1}^3$	$-0.9979x_{i,1}^3$
	$-x_{i,2}$	$-0.9861x_{i,2}$	$-1.3184x_{i,2}$	$-0.9975x_{i,2}$
			$1.3564x_{i,1}^2$	
			-88.3806	
			$-1.8841 \exp(x_{i,1})$	
$\mathbf{G}(x_i, x_j)$	$-(x_{j,1} - x_{i,1})$	$-0.9862(x_{j,1} - x_{i,1})$	$-22.6880(x_{j,1} - x_{i,1})$	$-1.0151(x_{j,1} - x_{i,1})$
			$-18.4197 \sin(x_{j,1} - x_{i,1})$	
			$181.6294\sigma(x_{j,1} - x_{i,1})$	

Table 6: Numerical results for FHN dynamics (randomly add 15% edges) in self-dynamics $\mathbf{F}(x_i)$ and interaction dynamics $\mathbf{G}(x_i, x_j)$ term by term (each term of true or inferred $\mathbf{G}(x_i, x_j)$ is understood to be divided by k_{in} , i.e., $\frac{\mathbf{G}(x_i, x_j)}{k_{\text{in}}}$, where k_{in} is the in-degree of node i).

	True Dynamics	Two-Phase	ARNI	FEX
$\mathbf{F}(x_i)$	$x_{i,1}$	$0.9828x_{i,1}$	$0.6644x_{i,1}$	$0.9835x_{i,1}$
	$-x_{i,1}^3$	$-0.9910x_{i,1}^3$	$-0.5332x_{i,1}^3$	$-1.0038x_{i,1}^3$
	$-x_{i,2}$	$-0.9837x_{i,2}$	$-1.2174x_{i,2}$	$-0.9916x_{i,2}$
			$-0.2063 \exp(x_{i,1})$	
			0.4520	
			$-0.2257x_{i,1}x_{i,2}$	
			$0.2303x_{i,1}^2x_{i,2}$	
			$-0.2061 \exp(x_{i,1})$	
$\mathbf{G}(x_i, x_j)$	$-(x_{j,1} - x_{i,1})$	$-0.9812(x_{j,1} - x_{i,1})$	$-0.9477(x_{j,1} - x_{i,1})$	$-1.0247(x_{j,1} - x_{i,1})$
			$-0.1134 \sin(x_{j,1} - x_{i,1})$	
			$0.6586\sigma(x_{j,1} - x_{i,1})$	
			0.4114 $x_{j,1}$	

Table 7: Numerical results for FHN dynamics (randomly delete 15% edges) in self-dynamics $\mathbf{F}(x_i)$ and interaction dynamics $\mathbf{G}(x_i, x_j)$ term by term (each term of true or inferred $\mathbf{G}(x_i, x_j)$ is understood to be divided by k_{in} , i.e., $\frac{\mathbf{G}(x_i, x_j)}{k_{\text{in}}}$, where k_{in} is the in-degree of node i).

Percent of edges perturbed	Two-Phase	ARNI	FEX
15% added	0.0082	0.8437	0.0049
15% deleted	0.0077	0.7192	0.0067

Table 8: sMAPE of FHN dynamics with 15% perturbed edges added or removed.

	True Dynamics	Two-Phase	ARNI	FEX
$\mathbf{F}(x_i)$	$x_{i,2}$	$0.9631x_{i,2}$	$0.6002x_{i,2}$	$0.9916x_{i,2}$
	$-x_{i,1}^3$	$-1.0039x_{i,1}^3$	$-1.3202x_{i,1}^3$	$-1.0023x_{i,1}^3$
	$3x_{i,1}^2$	$2.7820x_{i,1}^2$	$2.3557x_{i,1}^2$	$2.9659x_{i,1}^2$
	$-x_{i,3}$	$-0.9663x_{i,3}$	$-0.7982x_{i,3}$	$-0.9871x_{i,3}$
	3.24	2.9673	1.9699	3.2453
			$0.6597 \exp(x_{i,1})$	
$\mathbf{G}(x_i, x_j)$	$0.3\sigma(x_{j,1})$	$0.1529\sigma(x_{j,1})$	$0.2804\sigma(x_{j,1})$	$0.2963\sigma(x_{j,1})$
	$-0.15x_{i,1}\sigma(x_{j,1})$	$-0.0995x_{i,1}\sigma(x_{j,1})$	$-0.0847x_{i,1}\sigma(x_{j,1})$	$-0.1262x_{i,1}\sigma(x_{j,1})$

Table 9: Numerical results for Hindmarsh-Rose dynamics (SNR = 45) in self-dynamics $\mathbf{F}(x_i)$ and interaction dynamics $\mathbf{G}(x_i, x_j)$ term by term.

	True Dynamics	Two-Phase	ARNI	FEX
$\mathbf{F}(x_i)$	$x_{i,2}$	$0.9341x_{i,2}$	$0.3916x_{i,2}$	$0.9633x_{i,2}$
	$-x_{i,1}^3$	$-0.9948x_{i,1}^3$	$-1.0638x_{i,1}^3$	$-1.0058x_{i,1}^3$
	$3x_{i,1}^2$	$2.6599x_{i,1}^2$	$2.5882x_{i,1}^2$	$2.8923x_{i,1}^2$
	$-x_{i,3}$	$-0.9332x_{i,3}$	$-0.3871x_{i,3}$	$-0.9588x_{i,3}$
	3.24	3.1341	1.8715	3.2342
			$0.1318x_{i,2}x_{i,3}$	
			$0.2246 \exp(x_{i,2})$	
$\mathbf{G}(x_i, x_j)$	$0.3\sigma(x_{j,1})$	$0.1333\sigma(x_{j,1})$	None	$0.2683\sigma(x_{j,1})$
	$-0.15x_{i,1}\sigma(x_{j,1})$	None	None	$-0.1118x_{i,1}\sigma(x_{j,1})$
			$-0.2341\sigma(x_{j,1} - x_{i,1})$	

Table 10: Numerical results for Hindmarsh-Rose dynamics (SNR = 40) in self-dynamics $\mathbf{F}(x_i)$ and interaction dynamics $\mathbf{G}(x_i, x_j)$ term by term.

SNR	Two-Phase	ARNI	FEX
45	0.0924	0.2720	0.0158
40	0.2190	0.6252	0.0376

Table 11: sMAPE of HR dynamics with different levels of noise.

125 of the terms correctly when $\text{SNR} = 45$, with an extra term $0.6597 \exp(x_{i,1})$ in the self-dynamics.
126 Furthermore, the coefficients in the self-dynamics are poorly estimated, but it is interesting to
127 notice that the coefficients of interaction-dynamics are more accurate than those of Two-Phase,
128 owing again to ARNI's capability to infer the network structure. As for $\text{SNR} = 40$, ARNI infers
129 more redundant terms in self-dynamics, and it fails to identify both true terms in the original
130 dynamics, and incorrectly identifies a $-0.2341\sigma(x_{j,1} - x_{i,1})$ term. This shows that ARNI can
131 reasonably well infer most of the dynamics terms in low-noise case, while it fails to work as noise
132 level increases. Therefore, FEX has demonstrated its superior performance compared to Two-Phase
133 and ARNI to handle noisy data.